Ozonolysis can produce long-lived greenhouse gases from commercial refrigerants

Max Mcgillen, Zachary Fried, M. Anwar H. Khan, Keith Kuwata, Connor Martin, Simon O'doherty, Francesco Pecere, Dudley Shallcross, Kieran Stanley, Kexin Zhang

PNAS RESEARCH ARTICLE | EARTH, ATMOSPHERIC, AND PLANETARY SCIENCES

Ozonolysis can produce long-lived greenhouse gases from commercial refrigerants

Max R. McGillen[a,1], Zachary T. P. Fried[b], M. Anwar H. Khan[c], Keith T. Kuwata[d], Connor M. Martin[e], Simon O'Doherty[c], Francesco Pecere[f], Dudley E. Shallcross[c], Kieran M. Stanley[c], and Kexin Zhang[g]

Edited by Marsha Lester, University of Pennsylvania, Philadelphia, PA; received July 25, 2023; accepted October 30, 2023

Hydrofluoroolefins are being adopted as sustainable alternatives to long-lived fluorine- and chlorine-containing gases and are finding current or potential mass-market applications as refrigerants, among a myriad of other uses. Their olefinic bond affords relatively rapid reaction with hydroxyl radicals present in the atmosphere, leading to short lifetimes and proportionally small global warming potentials. However, this type of functionality also allows reaction with ozone, and whilst these reactions are slow, we show that the products of these reactions can be extremely long-lived. Our chamber measurements show that several industrially important hydrofluoroolefins produce CHF_3 (fluoroform, HFC-23), a potent, long-lived greenhouse gas. When this process is accounted for in atmospheric chemical and transport modeling simulations, we find that the total radiative effect of certain compounds can be several times that of the direct radiative effect currently recommended by the World Meteorological Organization. Our supporting quantum chemical calculations indicate that a large range of exothermicity is exhibited in the initial stages of ozonolysis, which has a powerful influence on the CHF_3 yield. Furthermore, we identify certain molecular configurations that preclude the formation of long-lived greenhouse gases. This demonstrates the importance of product quantification and ozonolysis kinetics in determining the overall environmental impact of hydrofluoroolefin emissions.

hydrofluoroolefin | ozonolysis | Criegee intermediate | global warming potential | fluoroform

Significance

As societies phase-out long-lived and polluting halocarbons in favor of shorter-lived alternatives, novel chemicals are entering our environment. Hydrofluoroolefins (HFOs) are one such alternative. HFOs react rapidly with OH, the main atmospheric oxidant, implying minimal global warming potentials (GWPs). However, their olefinic bond also affords a reaction with ozone. We measured the reactivity of five HFOs towards ozone, three of which were found to produce an extremely long-lived by-product, trifluoromethane. When these data are included in an atmospheric chemical transport model, GWPs are shown to increase several-fold, especially over longer time-horizons, demonstrating that a seemingly minor oxidation channel can be impactful.

Since their first commercial production in the 1930s, fluorinated gases (F-gases) have found many applications. First-generation F-gases, the chlorofluorocarbons (CFCs), presented low toxicity/flammability alternatives to incumbent refrigerants but depleted stratospheric ozone catastrophically (1) and their long atmospheric lifetimes and high radiative efficiency led to large global warming potentials (GWPs) (2). CFCs were replaced by hydrochlorofluorocarbons (HCFCs) and hydrofluorocarbons (HFCs) that possessed much smaller or negligible ozone depletion potentials (ODPs), but their long atmospheric lifetimes (hundreds of years in some cases) also resulted in high GWPs (2). In recognition of this, the Kigali amendment to the Montreal Protocol will precipitate the phase-down of these chemicals, which will be replaced by shorter-lived alternatives (3).

Hydrofluoroolefins (HFOs) represent a promising alternative to HFCs, since their olefinic bond reacts rapidly with hydroxyl radicals in the atmosphere, leading to short lifetimes of days to weeks. These reactions generate carbonyl products, which readily hydrolyze, prompting removal from the atmosphere (4), and these products are therefore unimportant in determining overall GWPs of HFOs (5).

However, olefinic bonds also react with ozone (O_3) and despite possessing much smaller rate coefficients, higher atmospheric mixing ratios of O_3 allow ozonolysis to act as a sink for HFOs in the environment. The ozonolysis mechanism is distinguished by its production of Criegee intermediates (CIs), energy-rich transient species that can participate in a multitude of unimolecular and bimolecular reactions (6), some of which could yield extremely long-lived products.

Previous studies on alkene ozonolysis have identified reaction channels that lead to the formation of short-chain hydrocarbons (7–10). Methane (CH_4) production in these systems is attributed to the "hot acid" channel, which operates when the acetaldehyde oxide CI engages in 1,3-ring closure forming 3-methyldioxirane, which isomerizes to acetic acid, formed with sufficient internal energy that it decomposes toward CH_4 and CO_2 via decarboxylation (Scheme 1) (11) Here, we propose that an analogous CHF_3-producing mechanism occurs for 2,2,2-trifluoroacetaldehyde oxide (TFAO), a CI that is produced in the ozonolysis of a subset of HFOs possessing substitution of CF_3 and hydrogen onto the same olefinic carbon atom, a commonplace motif among commercial F-gases, e.g., HFO-1234ze(*E*/*Z*), HCFO-1233zd(*E*/*Z*), HFO-1336mzz(*E*/*Z*), HFO-1243zf, and HFO-1354mzy(*E*/*Z*).

Author contributions: M.R.M. designed research; M.R.M., Z.T.P.F., M.A.H.K., K.T.K., C.M.M., S.O., F.P., D.E.S., K.M.S., and K.Z. performed research; M.R.M. analyzed data; and M.R.M., M.A.H.K., K.T.K., S.O., D.E.S., and K.M.S. wrote the paper.

The authors declare no competing interest.

This article is a PNAS Direct Submission.

[1]To whom correspondence may be addressed. Email: max.mcgillen@cnrs-orleans.fr.

This article contains supporting information online at https://www.pnas.org/lookup/suppl/doi:10.1073/pnas.2312714120/-/DCSupplemental.

Published December 11, 2023.

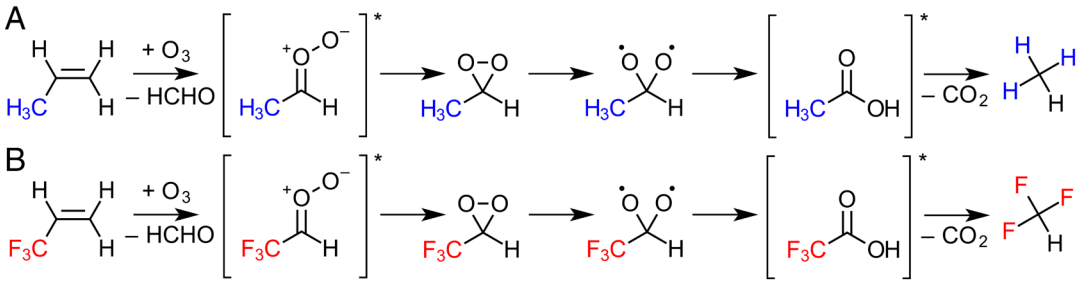

Scheme 1. Reaction sequence (*A*) is a simplified representation of the "hot acid" channel in the ozonolysis of propene, resulting in the production of methane from the decarboxylation of acetic acid. Reaction sequence (*B*) represents an analogous sequence, whereby CHF_3 is produced from thermally excited trifluoroacetic acid.

Furthermore, for HFOs possessing similar substitution patterns containing longer-chain fluorinated groups, analogous reactions are expected to occur, leading to other long-lived F-gases. Fig. 1 shows a schematic potential energy surface (PES) for the ozonolysis of HFO-1234ze(*E*) ($CHF{=}CHCF_3$), a complex potential energy landscape with a high degree of exothermicity, punctuated by a series of potential energy wells, culminating in CHF_3 and CO_2 formation.

Results

To assess the potential of HFO ozonolysis as a source of long-lived F-gases in the atmosphere, a combination of experiment, theory, and global modeling simulations were performed, allowing us to determine product yields, rationalize the underlying chemical mechanisms and estimate the environmental consequences.

In the experimental phase, several chamber experiments were conducted where CHF_3 yields from the ozonolysis of different HFOs were determined. Experiments consisted of simultaneous high-precision monitoring of HFO consumption and CHF_3 production using the Medusa preconcentration gas chromatography-mass spectrometry technique (12). To assess atmospheric loss rates of HFOs toward O_3, we determined gas-phase ozonation* rate coefficients for HFO-1234yf, HCFO-1233xf, HFO-1243zf, HFO-1336mzz(*Z*), and HFO-1234ze(*E*) using relative and absolute methods (Fig. 2 and *SI Appendix*, Table S2).

The slow ozonation rates exhibited by these HFOs require a large O_3 excess (>100 ppm) to be present in the chamber for long durations—several days for slower reactions, it is therefore imperative that background O_3 losses are exceptionally low such that bimolecular loss through reaction with HFOs remains competitive. The chamber apparatus has been described elsewhere (18–20), with the experimental protocol being adapted to reduce additional O_3 losses, which were minimized by conditioning chamber surfaces with high O_3 concentrations prior to experiments.

Because ozonolysis reactions produce several reactive by-products such as OH and stabilized Criegee intermediates (SCIs), large scavenger concentrations were employed to remove these species. Isopropanol was favored as it reacts rapidly with OH (21) and by analogy to similar systems, will also scavenge SCIs (22–25). Regarding OH, HO_2 is produced from subsequent reactions with oxygen, but this is not expected to react significantly with haloolefins (26) and will be lost primarily to self-reaction yielding H_2O_2, or reaction with O_3, yielding OH (22). Regarding SCIs, hydroperoxide adducts are expected to form (23), analogous to other systems (27–29). Consistent results were obtained for other scavengers (e.g., combinations of cyclohexane and formic acid).

Of the HFOs studied, three produced quantifiable CHF_3-yields. Fig. 2 shows CHF_3-yield data for HFO-1243zf ($CH_2{=}CHCF_3$), HFO-1234ze(*E*) (*trans*-$CHF{=}CHCF_3$), and HFO-1336mzz(*Z*) (*cis*-$CF_3CH{=}CHCF_3$). High linearity, precision, and reproducibility between experiments were observed in each case, with similar CHF_3-yields (0.37 ± 0.02 and 0.42 ± 0.02%) exhibited by HFO-1243zf and HFO-1336mzz(*Z*), respectively. Surprisingly, HFO-1234ze(*E*) showed substantially larger yields (3.11 ± 0.05%) than HFO-1336mzz(*Z*) despite it being an asymmetrical alkene with less than unit yield of TFAO. This indicates that the branching of primary ozonide fragmentation is not the primary determinant in CHF_3 production and that energy partitioning upon cycloreversion and energy transfer of key intermediates play important roles. We also performed experiments upon HFO-1234yf and HCFO-1233xf to investigate the possible production of CF_4 and CF_3Cl through analogous reactions. We found no observable production of these long-lived species, nor any CHF_3 production, suggesting that this process is limited to H-migration from the carbon vicinal to the CF_3 group.

To understand this process further, we performed quantum calculations on ozonolysis potential energy surfaces (PES) of three CHF_3-producing HFOs: 1234ze(*E*), 1243zf, and 1336mzz(*Z*) using the ωB97X-D/cc-pVTZ model chemistry (30) implemented in Gaussian 16 (31), followed by master equation calculations using MultiWell-2019 (32–34), for further details, see *SI Appendix*. Fig. 1 provides an overview of CHF_3 production on the PES of HFO-1234ze(*E*) ozonolysis. The reaction proceeds through a van der Waals complex, representing a shallow energy well on the PES, which is not expected to affect the kinetics under tropospheric conditions. Next, a small barrier (~6 kcal mol^{-1}) to forming the primary ozonide (POZ) is encountered. This is a highly exothermic reaction step (~–60 kcal mol^{-1}), and although no collisional stabilization of POZ is predicted, some energy transfer with the bath gas is anticipated. The POZ undergoes cycloreversion leading to two CIs with a CF_3 substituent: *syn*- and *anti*-TFAO. Qualitatively, trends in CHF_3-yields follow trends in the energies of cycloreversion transition states. The two leading to TFAO are 5–8 kcal mol^{-1} lower in energy than those leading to CIs with an F substituent (*SI Appendix*, Scheme S1). This corresponds to yields of *syn*- and *anti*-TFAO that are 10 times larger, with simulations predicting a total TFAO yield of 0.906. TFAO will be present in both chemically activated (i.e., "excited") and stabilized forms, both of which participate in sequential unimolecular reactions, the relative populations of each depending upon bath gas pressure.

First, HFO-1234ze(*E*) ozonolysis is considered. As with all systems described here, the fate of excited TFAO is of primary importance in determining CHF_3 yields, and we begin with this. For both *syn*- and *anti*-TFAO, 1,3-ring closure toward 3-trifluoromethyldioxirane

*We use "ozonation" here instead of the more commonly used "ozonolysis." Ozonation is a broader term that can apply to any mechanism of reaction between O_3 and an alkene. Ozonolysis refers strictly to the 1,3-cycloaddition of ozone across an olefinic bond.

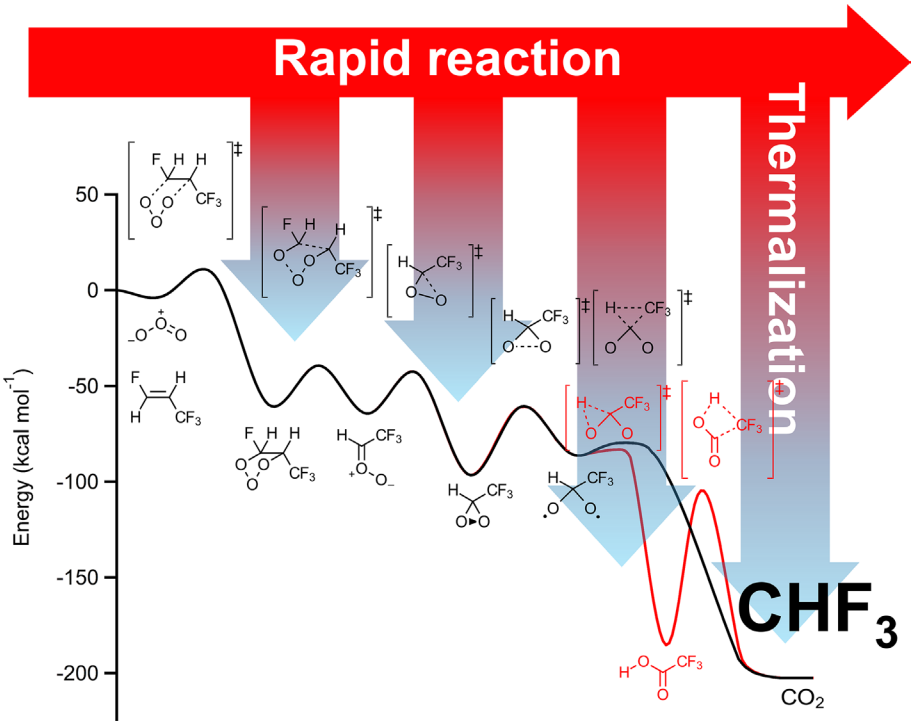

Fig. 1. Potential energy surface for the ozonolysis of a popular commercial refrigerant, HFO-1234ze(*E*). The formation of CHF_3, a potent greenhouse gas, is formed through two energetically favorable reaction channels. The CHF_3-yield is determined by the energy content of key reaction intermediates and the competition between unimolecular rearrangements and collisional deactivation. For simplicity, parallel non-CHF_3-producing channels are not presented.

dominates. Analogous to theoretical results of other ozonolysis systems (35–37), we predict that 3-trifluoromethyldioxirane undergoes O–O bond homolysis, forming the bis(oxy) diradical, which decomposes directly via double β-scission to CHF_3 + CO_2, or rearranges in a 1,2-H shift, yielding trifluoroacetic acid (TFA). Some TFA is sufficiently chemically activated (i.e., "hot") that it decomposes, yielding CHF_3 + CO_2 indirectly through decarboxylation (*SI Appendix*, Schemes S2 and S3). Direct and indirect CHF_3 yields are affected by the barrier heights of these two channels and also the internal energy of TFA. Master equation simulations show the proportion of indirect to direct CHF_3 production is ~2:1, which is qualitatively consistent with transition states (TS) leading to TFA being ~4 kcal mol^{-1} lower in energy than corresponding TSs leading directly to CHF_3. The remaining TFAO is present as SCI, either formed "cold" or subsequently stabilized by the bath gas. The pressure dependence of the stabilized *syn*-TFAO yield is shown in Fig. 3, where SCI yields increase from ~5 to 40% from 0 to 800 Torr. Lower yields (~2–20%) are observed for *anti*-TFAO, which possesses more internal energy, being formed from a combination of a higher barrier cycloaddition channel and a lower barrier cycloreversion channel than its *syn* counterpart.

Stabilized TFAO is far less efficient at producing CHF_3. Similar to excited TFAO—and excluding bimolecular reactions—1,3-ring closure towards 3-trifluoromethyldioxirane dominates, with 298 K isomerization rates of 5.21×10^{-3} and 1.30×10^{-2} s^{-1} for *syn*- and *anti*-TFAO, respectively. However, depending on reaction rates with various hydrogenous species present in the atmosphere, e.g., H_2O, $(H_2O)_2$, R(O)OH, ROH, SCIs may be lost toward bimolecular processes, producing various hydroperoxides. In our experiments, [isopropanol] was sufficient to effectively titrate stabilized TFAO, with estimated first-order loss rates of ~5×10^2 s^{-1}, assuming rate coefficients similar to that of CH_2OO with alcohols (23). As with excited CI, upon ring closure, dioxirane is formed. However, 3-trifluoromethyldioxirane may be collisionally stabilized in yields of 61 to 74% from the *syn*- and *anti*-TFAO, respectively, at 760 Torr. Homolysis of this stabilized dioxirane becomes negligibly slow (1.96×10^{-13} s^{-1}), indicating that it is only chemically activated dioxirane that can form CHF_3. The stability of 3-trifluoromethyldioxirane raises the intriguing possibility that ozonolysis results in several novel species which may persist on the timescales of bimolecular reactions. In this regard, fluorinated oxiranes are found to be potent oxidants in laboratory settings, where they efficiently insert into saturated and unsaturated reaction sites (38). The total calculated CHF_3-yield for HFO-1234ze(*E*), 0.636, is shown in *SI Appendix*, Table S4.

Second, HFO-1243zf ozonolysis is considered. Similar to HFO-1234ze(*E*), this reaction forms excited TFAO, which largely controls CHF_3 yields. However, cycloreversion of the primary ozonide formed in HFO-1243zf ozonolysis differs from that in HFO-1234ze(*E*) in two important ways: 1) The barriers to forming TFAO are now 5 to 8 kcal mol^{-1} higher in energy than the barriers to forming CH_2OO, which cannot ultimately form CHF_3. 2) The transition states leading to TFAO are 12 to 13 kcal mol^{-1} higher than the analogous transition states of HFO-1234ze(*E*). According to the statistical rate theory of Forst (39) this means that the TFAO formed in HFO-1243zf ozonolysis has lower internal energies. Since CHF_3 production depends on both yields of TFAO and the internal energy with which it is formed, a reduced yield of CHF_3 of 0.022 from HFO-1243zf ozonolysis is anticipated from our calculations.

Third, HFO-1336mzz(*Z*) ozonolysis is considered. The symmetrical structure of this alkene is such that ozonolysis leads to the highest (i.e., unit) yield of TFAO. Since each TFAO formed has the potential to produce CHF_3, intuitively, it might be expected to have correspondingly high yields of CHF_3. However, there are several factors that contribute to this not being the case. 1) Upon formation, the POZ, which is substituted with two CF_3 groups, possesses more heavy atoms and a larger collisional cross-section than the other POZs considered here and is therefore

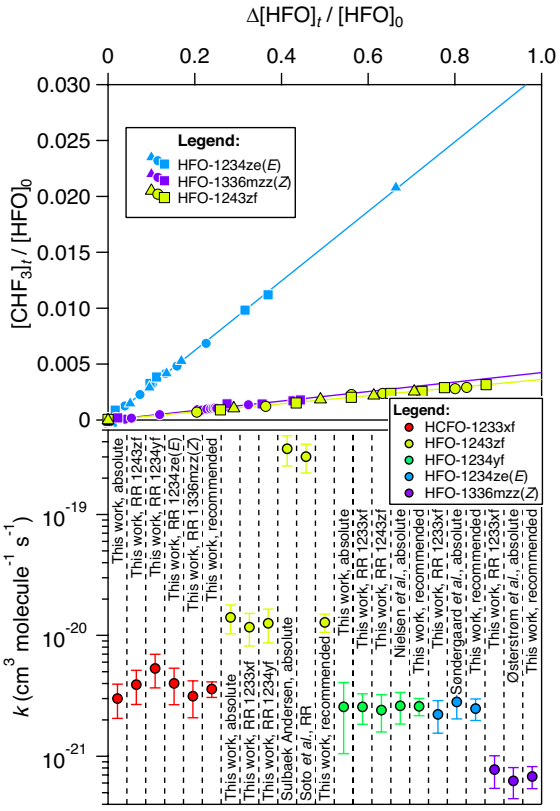

Fig. 2. *Upper* panel: experimentally determined CHF_3-yields from HFO-1234ze(*E*), HFO-1243zf, and HFO-1336mzz(*Z*) ozonolysis reactions. Different symbols are used to distinguish separate experiments, demonstrating the precise reproducibility of these data. *Lower* panel: ozonation rate coefficients of the various haloalkenes considered in this work at 296 K together with available room temperature literature measurements. Excellent consistency is observed between absolute and relative measurements in most cases (13–15), with the exception of two literature values for HFO-1243zf, which are significantly larger than the values reported here (16, 17).

more prone to energy transfer with the bath gas and vibrational relaxation, broadly consistent with previous calculations (40). 2) Energies of the cycloreversion transition states are similar to those encountered in HFO-1243zf (*SI Appendix*, Scheme S5), leading to higher yields of stabilized TFAO (possessing much lower CHF_3-yields). The final calculated yield of CHF_3 is 0.021.

By comparing experimental CHF_3-yields with calculations (*SI Appendix*, Table S4), we find that although the order of CHF_3-yields is consistent: HFO-1243zf ≈HFO-1336mzz(*Z*)<HFO-1234ze(*E*), calculations lead to overestimations of CHF_3-yields. Differences could arise from uncertainties in rates of POZ cycloreversion, for example, underplaying the importance of energy transfer with the bath gas. Other differences could result from not considering reaction channels that compete with ozonolysis, such as epoxidation, which can operate in electron-poor alkenes (41). It appears that vinyl halogen substitutions may be a particularly important consideration in these reactions, which may explain why we see the greatest disparity between calculation and experiment in the case of HFO-1234ze(*E*). Therefore, it may be necessary to perform follow-up experiments to investigate this possibility in HFOs. Nevertheless, as a qualitative indicator of CHF_3 production, these calculations provide insight into the factors that control this yield: the regioselectivity of POZ formation and cycloreversion, which affects yield, conformation, and energy content of the CHF_3-precursor, TFAO; and collisional stabilization of the POZ and TFAO by the bath gas. Furthermore, they confirm our experimental findings that the "hot acid" channel operates beyond the strictly hydrocarbon systems that have been described previously (7–10).

Discussion

To evaluate the atmospheric implications of these results, the kinetic data of this study were incorporated into global chemistry and transport simulations (*SI Appendix*), where competitive losses of HFOs toward OH and O_3 were assessed. Wet and dry deposition was neglected in the model since neither is expected to contribute significantly to this class of compound (42). Furthermore, despite a potentially important influence of temperature and pressure upon collisional stabilization in these reactions, in the absence of quantitative experimental data, we have not included these in our model treatment. Model runs showed that most (~65%) HFO loss by ozonation occurs from 0 to 3 km, corresponding to 760–530 Torr. Our quantum and master equation calculations suggest that over this pressure range, yields are only mildly and negatively affected by pressure (Fig. 3), which will be offset to some extent by the positive temperature dependence of these reactions (*SI Appendix*,

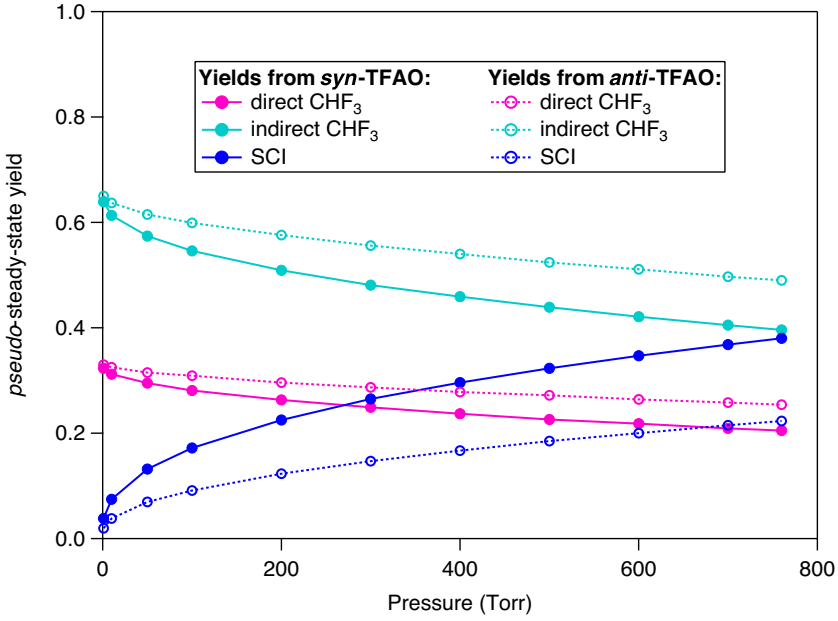

Fig. 3. Pressure dependences of the stabilized *syn* and *anti*-TFAO yields in HFO-1234ze(*E*) ozonolysis. Direct and indirect CHF_3 production occurs mainly through excited TFAO unimolecular reactions; therefore, collisional quenching serves to increase the SCI population and decrease the CHF_3-yield.

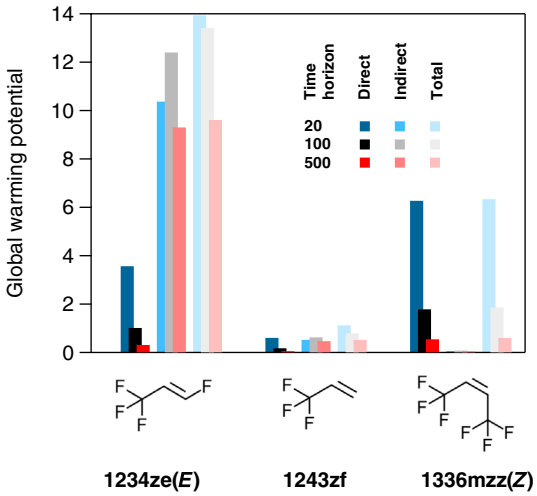

Fig. 4. The effects of CHF_3 formation on the calculated global warming potentials of several HFOs considered in this work. The largest effect can be seen for HFO-1234ze(*E*), whose indirect GWP is several times greater than the direct. It can also be seen how its GWP remains virtually unchanged between the 20- and 100-y time horizons and is also nonnegligible over the 500-y time horizon, in contrast to current assessments of the environmental impact of this HFO.

Table S5). In the absence of data, temperature dependence in the ozone reactions was not included in the model, whose expected positive temperature dependences would increase the fraction lost between 0 and 3 km and therefore reduce the importance of the pressure dependence of CHF_3 formation.

Fig. 4 shows the effects of including ozonolysis upon GWP calculations. For HFO-1234ze(*E*), which has the largest yield of CHF_3 studied, we find that the GWP associated with CHF_3 production is significantly larger than the primary GWP that is calculated based on radiative efficiency and atmospheric lifetime alone. Furthermore, the production of CHF_3 affects these calculations dramatically over longer time horizons. Although the radiative impacts of HFOs are typically not expected to last far beyond their atmospheric lifetimes (~10 d), when ozonolysis products are accounted for, HFO-1234ze(*E*) still has a significant GWP even at the 500-y time horizon.

The fractions of HFOs that are consumed by ozone compared with OH in our global simulations are minor in each case, contributing 2.96%, 1.25%, and 0.13% for HFO-1234ze(*E*), HFO-1243zf and HFO-1336mzz(*Z*), respectively. In some circumstances, the impact of ozonolysis will be higher than our simulations suggest, since large HFO emissions from the mobile air conditioning sector are expected in some of the world's most polluted regions (43), where OH can be suppressed by NO_x, leading to O_3/OH ratios that can be higher than global averages (44).

In conclusion, we present experiments and calculations showing that the environmental impact of certain mass-produced HFOs is significantly affected by reactions with O_3. Conventional approaches focus on lifetimes of emitted substances with respect to hydroxyl, the dominant atmospheric oxidant, sparing little attention to reactions with other oxidants and their products. We highlight a pitfall of such a reductionist approach, demonstrating clearly why knowledge of the atmospheric oxidation of molecules should extend beyond their initiation reactions with hydroxyl. Furthermore, we show that precise laboratory work and calculations are absolutely essential if industries are to correctly assess environmental impacts of new chemical products.

Materials and Methods

Details on the chamber experiments, including the measurement of absolute and relative ozonation rate coefficients, CHF_3 product yields, chemical analysis using the Medusa GC/MS technique can be found in *SI Appendix*, sections 1 and 2. Additional information on computational methods are provided in *SI Appendix*, section 3. A more detailed description of global chemistry and transport modeling, together with GWP calculations is given in *SI Appendix*, section 4.

Data, Materials, and Software Availability. All study data are included in the article and/or *SI Appendix*.

ACKNOWLEDGMENTS. M.R.M. Gratefully acknowledges the support from the Marie Skłodowska-Curie Individual Fellowship HOMER (702794). D.E.S. and M.A.H.K. were supported by NERC (NE/K004905/1), the Primary Science Teaching Trust, and Bristol ChemLabS. K.T.K., C.M.M., and F.P. acknowledge the support from the Environmental Chemical Sciences program of the NSF (CHE-2108202). C.M.M. and K.Z. acknowledge the support from the Beltmann Chemistry Research Fund of Macalester College. F.P. acknowledges the support from the Collaborative Summer Research Fund of Macalester College.

Author affiliations: [a]CNRS-Orléans, Institut de Combustion Aérothermique Réactivité et Environnement, Orléans 45071, France; [b]Department of Chemistry, Massachusetts Institute of Technology, Boston, MA 02139; [c]School of Chemistry, University of Bristol, Bristol BS8 1TS, United Kingdom; [d]Department of Chemistry, Macalester College, Saint Paul, MN 55105; [e]Department of Chemistry, University of California, Irvine, CA 92697; [f]Department of Chemistry, The Pennsylvania State University, State College, PA 16801; and [g]Department of Chemistry, Northwestern University, Evanston, IL 60208

1. M. J. Molina, F. S. Rowland, Stratospheric sink for chlorofluoromethanes: Chlorine atom-catalysed destruction of ozone. *Nature* **249**, 810–812 (1974).
2. World Meteorological Organization, Scientific assessment of ozone depletion: 2014. Pursuant to Article 6 of the Montreal Protocol on substances that deplete the ozone layer (2015).
3. The Kigali Amendment (2016): The Amendment to the Montreal Protocol Agreed by the Twenty-Eighth Meeting of the Parties (Kigali, 10-15 October 2016). https://ozone.unep.org/treaties/montreal-protocol/amendments/kigali-amendment-2016-amendment-montreal-protocol-agreed. Accessed 27 July 2023.
4. J. B. Burkholder, R. A. Cox, A. R. Ravishankara, Atmospheric degradation of ozone depleting substances, their substitutes, and related species. *Chem. Rev.* **115**, 3704–3759 (2015).
5. T. J. Wallington, M. P. Sulbæk Andersen, O. J. Nielsen, Atmospheric chemistry of short-chain haloolefins: Photochemical ozone creation potentials (POCPs), global warming potentials (GWPs), and ozone depletion potentials (ODPs). *Chemosphere* **129**, 135–141 (2015).
6. L. Vereecken, A. Novelli, D. Taraborrelli, Unimolecular decay strongly limits the atmospheric impact of Criegee intermediates. *Phys. Chem. Chem. Phys.* **19**, 31599–31612 (2017).
7. J. T. Herron, R. E. Huie, Stopped-flow studies of the mechanisms of ozone-alkene reactions in the gas phase propene and isobutene. *Int. J. Chem. Kinet.* **10**, 1019–1041 (1978).
8. E. C. Tuazon, S. M. Aschmann, J. Arey, R. Atkinson, Products of the gas-phase reactions of O_3 with a series of methyl-substituted ethenes. *Environ. Sci. Technol.* **31**, 3004–3009 (1997).
9. R. S. Disselkamp, M. Dupuis, A temperature-dependent study of the ozonolysis of propene. *J. Atmos. Chem.* **40**, 231–245 (2001).
10. R. Uchida, K. Sato, T. Imamura, Gas-phase ozone reactions with *Z*-3-hexenal and *Z*-3-hexen-1-ol: Formation yields of OH radical, propanal, and ethane. *Chem. Lett.* **44**, 457–458 (2015).
11. J. G. Calvert, Ed., *The Mechanisms of Atmospheric Oxidation of the Alkenes* (Oxford University Press, 2000).
12. T. Arnold *et al.*, Automated measurement of nitrogen trifluoride in ambient air. *Anal. Chem.* **84**, 4798–4804 (2012).
13. O. J. Nielsen *et al.*, Atmospheric chemistry of $CF_3CF{=}CH_2$: Kinetics and mechanisms of gas-phase reactions with Cl atoms, OH radicals, and O_3. *Chem. Phys. Lett.* **439**, 18–22 (2007).
14. R. Søndergaard, O. J. Nielsen, M. D. Hurley, T. J. Wallington, R. Singh, Atmospheric chemistry of *trans*-CF_3CHCHF: Kinetics of the gas-phase reactions with Cl atoms, OH radicals, and O_3. *Chem. Phys. Lett.* **443**, 199–204 (2007).
15. F. F. Østerstrøm, S. T. Andersen, T. I. Sølling, O. J. Nielsen, M. P. Sulbaek Andersen, Atmospheric chemistry of *Z*- and *E*-$CF_3CH{=}CHCF_3$. *Phys. Chem. Chem. Phys.* **19**, 735–750 (2017).
16. M. P. S. Andersen *et al.*, Atmospheric chemistry of $C_xF_{2x+1}CHCH_2$ (x=1, 2, 4, 6, and 8): Kinetics of gas-phase reactions with Cl atoms, OH radicals, and O_3. *J. Photoch. Photobio. A* **176**, 124–128 (2005).
17. A. Soto *et al.*, Kinetic and mechanistic study of the gas-phase reaction of $C_xF_{2x+1}CHCH_2$ (x=1, 2, 3, 4 and 6) with O_3 under atmospheric conditions. *Chemosphere* **201**, 318–327 (2018).
18. K. E. Leather, M. R. McGillen, C. J. Percival, Temperature-dependent ozonolysis kinetics of selected alkenes in the gas phase: An experimental and structure–activity relationship (SAR) study. *Phys. Chem. Chem. Phys.* **12**, 2935–2943 (2010).
19. K. E. Leather *et al.*, Acid-yield measurements of the gas-phase ozonolysis of ethene as a function of humidity using Chemical Ionisation Mass Spectrometry (CIMS). *Atmos. Chem. Phys.* **12**, 469–479 (2012).
20. M. R. McGillen, M. Ghalaieny, C. J. Percival, Determination of gas-phase ozonolysis rate coefficients of C_{8-14} terminal alkenes at elevated temperatures using the relative rate method. *Phys. Chem. Chem. Phys.* **13**, 10965–10969 (2011).

21. M. R. McGillen *et al.*, Database for the kinetics of the gas-phase atmospheric reactions of organic compounds. *Earth Syst. Sci. Data* **12**, 1203–1216 (2020).
22. J. B. Burkholder *et al.*, Chemical kinetics and photochemical data for use in atmospheric studies. Evaluation Number 18. JPL Publication 15-10 (2015). https://jpldataeval.jpl.nasa.gov/pdf/JPL_Publication_15-10.pdf. Accessed 27 July 2023.
23. M. R. McGillen *et al.*, Criegee intermediate–alcohol Reactions, a potential source of functionalized hydroperoxides in the atmosphere. *ACS Earth Space Chem.* **1**, 664–672 (2017).
24. S. V. Tadayon, E. S. Foreman, C. Murray, Kinetics of the reactions between the Criegee intermediate CH_2OO and alcohols. *J. Phys. Chem. A* **122**, 258–268 (2018).
25. Y.-H. Lin, K. Takahashi, J. J.-M. Lin, Reactivity of Criegee intermediates toward carbon dioxide. *J. Phys. Chem. Lett.* **9**, 184–188 (2018).
26. A. J. Hynes, R. C. Richter, C. J. Nien, Laser photofragmention-laser induced fluorescence detection of the hydroperoxyl radical: Photofragment energy distributions, detection sensitivity and kinetics. *Chem. Phys. Lett.* **258**, 633–638 (1996).
27. P. Neeb, O. Horie, G. K. Moortgat, The nature of the transitory product in the gas-phase ozonolysis of ethene. *Chem. Phys. Lett.* **246**, 150–156 (1995).
28. P. Neeb, O. Horie, G. K. Moortgat, Gas–phase ozonolysis of ethene in the presence of hydroxylic compounds. *Int. J. Chem. Kinet.* **28**, 721–730 (1996).
29. H. J. Tobias, P. J. Ziemann, Kinetics of the gas-phase reactions of alcohols, aldehydes, carboxylic acids, and water with the C13 stabilized Criegee intermediate formed from ozonolysis of 1-tetradecene. *J. Phys. Chem. A* **105**, 6129–6135 (2001).
30. J.-D. Chai, M. Head-Gordon, Long-range corrected hybrid density functionals with damped atom–atom dispersion corrections. *Phys. Chem. Chem. Phys.* **10**, 6615 (2008).
31. M. J. Frisch *et al.*, Gaussian 16, Revision C.01 (Gaussian, Inc., Wallingford, CT, 2016). https://gaussian.com/gaussian16/. Accessed 27 July 2023.
32. J. R. Barker, Multiple-Well, multiple-path unimolecular reaction systems. I. MultiWell computer program suite. *Int. J. Chem. Kinet.* **33**, 232–245 (2001).
33. J. R. Barker, Energy transfer in master equation simulations: A new approach. *Int. J. Chem. Kinet.* **41**, 748–763 (2009).
34. J. R. Barker, *et al.*, Multiwell-2019 Software Suite (University of Michigan, Ann Arbor, MI, 2019).
35. D. Cremer, E. Kraka, P. G. Szalay, Decomposition modes of dioxirane, methyldioxirane and dimethyldioxirane–A CCSD(T), MR-AQCC and DFT investigation. *Chem. Phys. Lett.* **292**, 97–109 (1998).
36. J. M. Anglada, J. M. Bofill, S. Olivella, A. Solé, Theoretical investigation of the low-lying electronic states of dioxirane: Ring opening to dioxymethane and dissociation into CO_2 and H_2. *J. Phys. Chem. A* **102**, 3398–3406 (1998).
37. T. L. Nguyen, H. Lee, D. A. Matthews, M. C. McCarthy, J. F. Stanton, Stabilization of the simplest Criegee intermediate from the reaction between ozone and ethylene: A high-level quantum chemical and kinetic analysis of ozonolysis. *J. Phys. Chem. A* **119**, 5524–5533 (2015).
38. R. Curci, A. Dinoi, M. F. Rubino, Dioxirane oxidations: Taming the reactivity-selectivity principle. *Pure Appl. Chem.* **67**, 811–822 (1995).
39. W. Forst, *Unimolecular Reactions: A Concise Introduction* (Cambridge University Press, 2003).
40. B. Chuong, J. Zhang, N. M. Donahue, Cycloalkene ozonolysis: Collisionally mediated mechanistic branching. *J. Am. Chem. Soc.* **126**, 12363–12373 (2004).
41. P. S. Bailey, "Chapter XI electrophilic ozone attack on olefins. Epoxides and other "partial cleavage" products" in *Ozonation in Organic Chemistry*, W. Trahanovsky, Eds. (Academic Press, 1978), pp. 197–222.
42. T. J. Wallington, J. E. Anderson, Comment on "Environmental fate of the next generation refrigerant 2,3,3,3-Tetrafluoropropene (HFO-1234yf)" . *Environ. Sci. Technol.* **49**, 8263–8264 (2015).
43. Z. Wang *et al.*, Impacts of the degradation of 2,3,3,3-tetrafluoropropene into trifluoroacetic acid from its application in automobile air conditioners in China, the United States, and Europe. *Environ. Sci. Technol.* **52**, 2819–2826 (2018).
44. T. K. Starn *et al.*, Observations of isoprene chemistry and its role in ozone production at a semirural site during the 1995 Southern Oxidants Study. *J. Geophys. Res.* **103**, 22425–22435 (1998).